Hindawi
Advances in Materials Science and Engineering
Volume 2019, Article ID 4536268, 9 pages
https://doi.org/10.1155/2019/4536268

Research Article

The Effect of CuO on the Thermal Behavior of the High-Energy Combustion Agent of the Al/MnO_2 System

Hao Wang, Tao Guo, Wen Ding, Miao Yao, Xiang Fang, and Jia-xing Song

College of Field Engineering, Army Engineering University, Hou Biaoying Road No. 88, Nanjing, Jiangsu 210007, China

Correspondence should be addressed to Tao Guo; 1006230238@qq.com

Received 18 September 2018; Revised 9 December 2018; Accepted 18 December 2018; Published 3 April 2019

Academic Editor: Veronica Calado

In this work, the effect of CuO addition into the high-energy combustion agent of Al/MnO_2 system was studied. First, the combustion experiments of five samples with different contents had been carried out, in which CuO was found capable of influencing the flame ejection to a great extent. Then, in order to find out the underlying reasons, CuO effects on the thermal behavior of Al/MnO_2 system were analyzed via theoretical calculations of Gibbs free energy and enthalpy changes. In addition, field emission scanning electron microscopy (FE-SEM) that could characterize the mixture morphology and thermogravimetric-differential scanning calorimetry (TG-DSC) that could indentify the exothermic and endothermic reactions and measure mass change were carried out. Finally, on the basis of all experimental findings, it was suggested that addition of CuO into Al/MnO_2 system could result in dramatic increase of gas content throughout the reaction and the consequent high pressure. Also, speed of flame injection and heat released in the high-temperature area would thus be conducive to the continuous exothermic behavior of the reaction.

1. Introduction

Thermite is one of the high-test energy density agents that can supply a huge amount of chemical heat energy at a small dose [1–3]. Meanwhile, it possesses many other advantages such as rapid heat release, high adiabatic flame temperature, and excellent security. Thermite can be applied in a broad spectrum of fields such as metallurgy [4], welding [5], cutting [6], etc. Moreover, it is particularly popular in the destruction by unexploded ammunition due to its higher security, convenience, and portability, considering the principle that high energy combustion agent can burn up the warhead steadily via melting through the metal shell of ammunition [7]. When the traditional thermite is ignited by ignition agent, aluminum thermal reaction will be initiated to produce alumina and iron, commonly the mixture of aluminum and ferric oxide red powder at a ratio of 3 : 2. Then, a large amount of heat will be released simultaneously, which can increase the temperature up to 2000 K. Recently, the concept of thermite has been expanded beyond the traditional Al/Fe_2O_3 system, where other metal oxides like CuO, MnO_2, SiO_2, MoO_3, etc., [8–13] can replace iron oxide and cooperate with Al at a certain proportion. The obtained mixture is also known as thermites, for sufficient heat can be produced in the thermite reaction so as to melt the reduced metal at high temperature and harvest metal with higher purity. However, experimental studies [14] suggested that a small amount of slag together with an obvious area of flame jet could be generated when MnO_2 functioned as the oxidant. It would not impede the continuous heat transformation during combustion and improve combustion efficiency, contributing to some applications different from those involved the type of Al/Fe_2O_3.

Along with the rapid development of material science in recent years, much more attention has been paid to the research of micro- and nanoscale super thermites because the micro- and nanoscale energetic materials exhibit significantly increased overall performance, especially in the aspect of safety, compared with traditional energetic materials [10]. At present, a great deal of research studies have been carried out on the preparation, characterization, and application of super thermites made of micro- and nanoscale

materials. For example, Kim et al. [12] investigated the thermite reactions between Al/CuO nanowires and nanopowders through field emission scanning electron microscopy (FE-SEM) and energy dispersive spectroscopy (EDS), which suggested that the heat flow and energy release were examined specifically as well. According to Song et al. [15], the measurements on thermal properties and kinetics of Al/α-MnO_2 thermite with nanostructure indicated high heat release and low onset temperature.

Former sifting experiments suggested that the addition of CuO could exert a positive effect on the high-energy combustion agent of Al/MnO_2 thanks to the more powerful flame and the faster speed. However, common sense tells that the type Al/CuO agent can trigger deflagration-to-detonation transition (DDT) [16] during combustion processes.

It remains unclear how CuO can affect the combustion process when it collaborates as an additive with the type Al/MnO_2 agent, especially whether CuO can improve the combustion speed of the whole system. To this end, it is of great significance to investigate the effect of CuO on the combustion system which is composed of type Al/MnO_2 high-energy combustion agent.

2. Experimental

2.1. Materials. All chemicals were of analytical reagent grade and used directly without further treatment or purification, among which Al (the mass fraction of active Al was more than 99.8%), MnO_2, and CuO were supplied by Naiou Nanotechnology Co., Ltd., (Shanghai, China) while C_2H_6O was purchased from Sinopharm Chemical Regent Co., Ltd., (Shanghai, China).

2.2. Sample Preparation. Samples were prepared based on a total mass of 5 g, and specific contents of each raw material were calculated individually. CuO content was preset as 0, 5%, 10%, 15%, and 20%, while Al and MnO_2 were configured according to the minimum principle of Gibbs free energy. Detailed preparation steps are as follows. Dispersion of reagents in anhydrous ethanol was stirred cautiously and subjected to ultrasonic wave concussion for about 1 h. The obtained mixture was then transferred into evaporating dishes and dried at 60°C in vacuo for 18 h. Black gray solid was scraped carefully from the dishes afterwards, transferred to a mortar, and got ground into powders.

Finally, the weight percent of all samples were measured, as listed in Table 1.

2.3. Combustion Experiments. In this study, steel plates with thickness of 5 mm were utilized in the penetration test. The experimental settings were placed under the steel plate for loading various samples of high-energy combustion agent (Figure 1). Electric ignition was adopted for this experiment device.

2.4. Theoretical Calculation. The Eyring equation (also known as Eyring–Polanyi equation) describes the variation of a chemical reaction rate against temperature in chemical kinetics studies [17]. Complying with the transition state theory (i.e., activated-complex theory), this equation is basically equivalent to the empirical Arrhenius equation, both of which are readily derived from the statistical thermodynamics in the kinetic theory of gases. The general form of Eyring–Polanyi equation resembles that of the Arrhenius equation [18]:

$$k = \frac{k_B T}{h} e^{\Delta^{\ddagger} S^{\ominus}/R} e^{-\left(\Delta^{\ddagger} H^{\ominus}/RT\right)}, \quad (1)$$

which can be expressed as

$$k = \frac{k_B T}{h} e^{\Delta^{\ddagger} G^{\ominus}/RT}, \quad (2)$$

where k stands for reaction rate constant, T for absolute temperature, k_B for Boltzmann constant, h for Planck's constant, R for gas constant, and ΔG for Gibbs energy of activation (negative value).

The thermochemical software, HSC Chemistry, was applied for parameter calculation in the mathematical model of all mixtures at varied temperatures, including entropy change, enthalpy change, Gibbs free energy change, etc.

2.5. Morphology Characterization. Morphologies, particle sizes, and mixing situation of the samples were characterized on a field emission scanning electron microscope (FE-SEM, HITACHI High-Technologies Co., S-4800 II, Japan).

2.6. Thermal Analysis. Thermal properties were analyzed by TG-DSC (NETZSCH STA 449F3, Germany). Samples weighed about 15–25 mg were loaded in a corundum crucible and heated from 20°C to 1000°C at the heating rate of 10°C·min^{-1} under argon protection.

Table 1: Samples and corresponding formulations used for experiments.

No.	Weight percent (%)		
	Al	MnO_2	CuO
1#	29.27	70.73	0.00
2#	28.59	66.32	5.09
3#	27.95	62.09	9.95
4#	27.29	57.77	14.94
5#	26.62	53.46	19.92

3. Results and Discussion

3.1. Results of Combustion Experiments. Figure 2 presents the combustion processes where samples 1#–5# were ignited, respectively, and the resulting steel plates ablated by thermite are demonstrated in Figure 3. The reactions in all sets of experiments were extremely intense accompanied with bright flame, dazzling white light, dark smoke, and a little noise. As shown in the photographs below, with mounting content of CuO, the combustion process of thermite became increasingly violent. Meanwhile, the steel plates were destroyed much more seriously, which could even be melted at higher CuO content of 15% and 20% (4# and 5#), and then

(a) (b) (c)

Figure 1: Schematic demonstration (a) and actual photographs (b, c) of steel plates ablated by thermite. (a) Sketch map. (b) Physical map 1. (c) Physical map 2.

(a) (b) (c) (d) (e)

Figure 2: The combustion processes of thermite. (a) 1#. (b) 2#. (c) 3#. (d) 4#. (e) 5#.

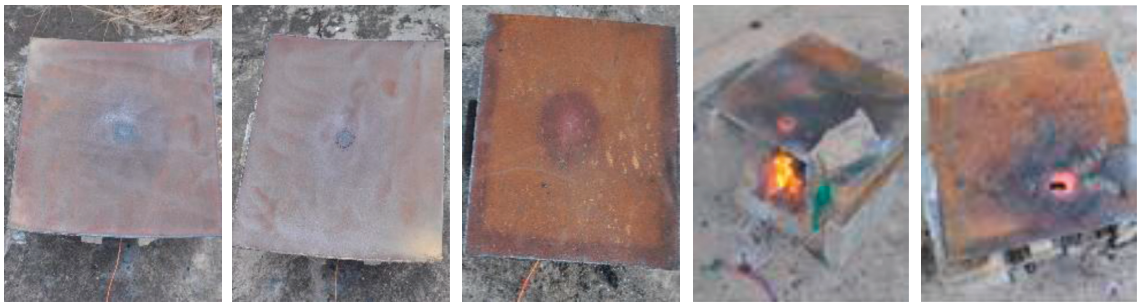

(a) (b) (c) (d) (e)

Figure 3: The resulting steel plates ablated by thermite. (a) 1#. (b) 2#. (c) 3#. (d) 4#. (e) 5#.

the flame heights reached 0.8 m and 1.1 m approximately after the steel plate was penetrated in those cases.

3.2. Results of Calculation. The reaction Gibbs free energy and the enthalpy of reaction were calculated by HSC Chemistry software. HSC Chemistry software combines various chemical reaction equations, including thermodynamics. It can simulate the traditional thermodynamic calculation under different temperatures, pressures, and concentrations in most cases and can be used in personal computers. HSC Chemistry 6.0, as the most downloaded version, is widely used in science education, industry, and research. HSC Chemistry 6.0 also plays an active role in chemical practice and research.

HSC Chemistry 6.0 contains many functions and submodules, and here we chose to use its "reaction calculation" module to simulate the parameters of the relevant thermochemical reactions, and ultimately, we got the Gibbs self-energy and chemical reaction enthalpy values from 0 to 1500°C. Then, the Arrhenius formula and Eyring equation can be found on the right. The burning rate and heat release of the flame type high-energy combustion agent were evaluated. The software interface of HSC Chemistry could be found as Figure 4 and the values of Gibbs free energy and enthalpy changes of five samples could be found in Tables 2 and 3.

It can be seen from Figure 5 that the absolute value of Gibbs free energy decreased gradually with the rising temperature for all the five samples, and decreasing rates

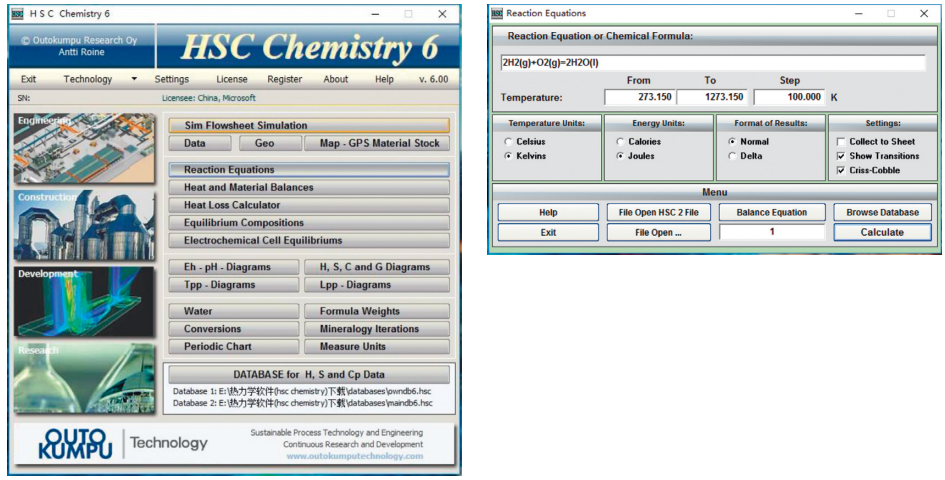

(a) (b)

Figure 4: The software interface of HSC Chemistry.

Table 2: Gibbs free energy of five samples.

Temperature (°C)	Absolute values of Gibbs free energy (kJ·mol^{-1})				
	$Al + MnO_2$	$Al + MnO_2 + CuO$ 5%	$Al + MnO_2 + CuO$ 10%	$Al + MnO_2 + CuO$ 15%	$Al + MnO_2 + CuO$ 20%
0.000	−956.591	−948.912	−939.981	−931.104	−921.698
100.000	−952.489	−944.908	−936.079	−927.303	−917.996
200.000	−948.061	−940.571	−931.840	−923.159	−913.944
300.000	−943.503	−936.095	−927.454	−918.860	−909.728
400.000	−938.927	−931.592	−923.030	−914.513	−905.454
500.000	−934.364	−927.091	−918.600	−910.150	−901.152
600.000	−929.790	−922.568	−914.139	−905.747	−896.801
700.000	−924.202	−917.046	−908.693	−900.373	−891.493
800.000	−917.477	−910.389	−902.118	−893.874	−885.064
900.000	−910.807	−903.778	−895.578	−887.401	−878.650
1000.000	−904.171	−897.193	−889.059	−880.941	−872.243
1100.000	−897.603	−890.686	−882.628	−874.580	−865.946
1200.000	−891.459	−884.681	−876.771	−868.867	−860.368
1300.000	−886.249	−879.240	−871.124	−863.002	−854.278
1400.000	−881.770	−874.364	−865.880	−857.376	−848.264
1500.000	−877.380	−869.561	−860.697	−851.796	−842.280

Table 3: Enthalpy changes of five samples.

Temperature (°C)	Enthalpy changes (kJ·mol^{-1})				
	$Al + MnO_2$	$Al + MnO_2 + CuO$ 5%	$Al + MnO_2 + CuO$ 10%	$Al + MnO_2 + CuO$ 15%	$Al + MnO_2 + CuO$ 20%
0.000	−967.169	−959.215	−949.999	−940.838	−931.153
100.000	−968.541	−960.606	−951.405	−942.261	−932.596
200.000	−969.443	−961.541	−952.367	−943.253	−933.622
300.000	−969.746	−961.894	−952.766	−943.700	−934.122
400.000	−969.678	−961.892	−952.824	−943.823	−934.314
500.000	−969.648	−961.935	−952.935	−944.004	−934.570
600.000	−969.820	−962.181	−953.250	−944.392	−935.034
700.000	−993.139	−985.068	−975.677	−966.364	−956.553
800.000	−989.230	−981.473	−972.388	−963.387	−953.891
900.000	−988.859	−981.190	−972.188	−963.273	−953.868
1000.000	−988.426	−980.838	−971.912	−963.078	−953.757
1100.000	−984.414	−975.420	−965.160	−954.958	−944.270
1200.000	−979.988	−971.323	−961.385	−951.511	−941.153
1300.000	−957.449	−956.577	−954.114	−951.881	−949.157
1400.000	−955.938	−955.315	−953.092	−951.105	−948.631
1500.000	−954.477	−954.097	−952.106	−950.359	−948.127

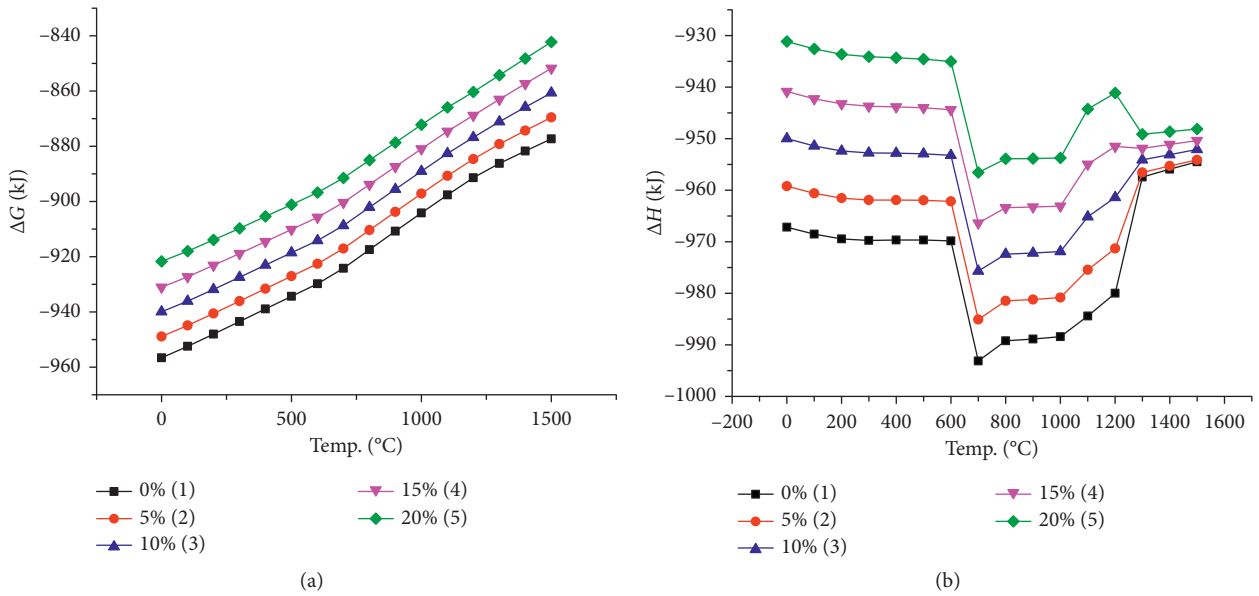

Figure 5: Changes of Gibbs free energy and enthalpy for the five samples.

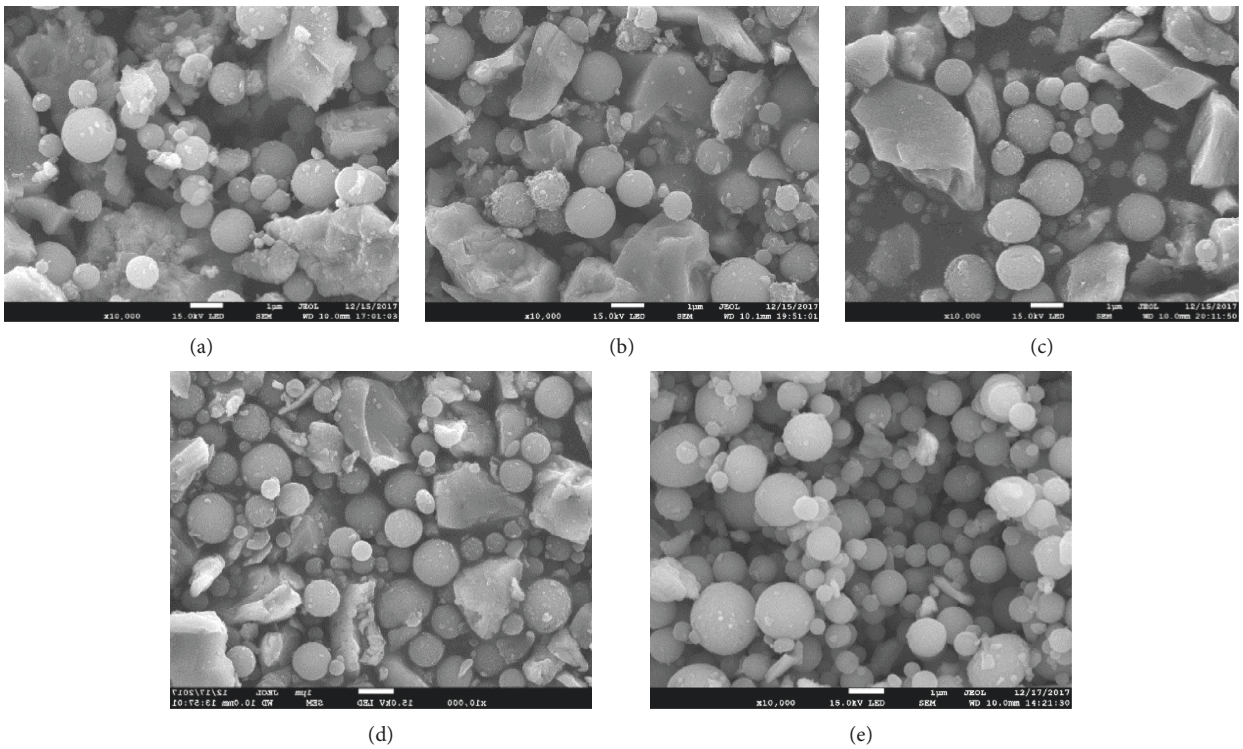

Figure 6: FE-SEM images of different samples. (a) 1#. (b) 2#. (c) 3#. (d) 4#. (e) 5#.

(slope) were calculated to be about 0.05 kJ/°C, which suggested an increasing k (reaction rate constant) at higher temperature according to the Eyring equation. On the other hand, samples with greater content of CuO exhibited smaller absolute value of Gibbs free energy at a certain temperature, thus lower k values could be obtained from the Eyring equation. Calculations suggested that the absolute value of Gibbs free energy decreased by 6~8 kJ after each 5% increase of CuO content.

Enthalpy change of the reaction resembled the first law of thermodynamics to some extent:

$$\Delta U = U_1 - U_2, \tag{3}$$

where U_1 is the initial state of heat energy and U_2 is the final state of heat energy.

The law states that a reaction with larger enthalpy will lead to more heat release. Variation in enthalpy change along with the combustion process could be observed from Figure 4 as

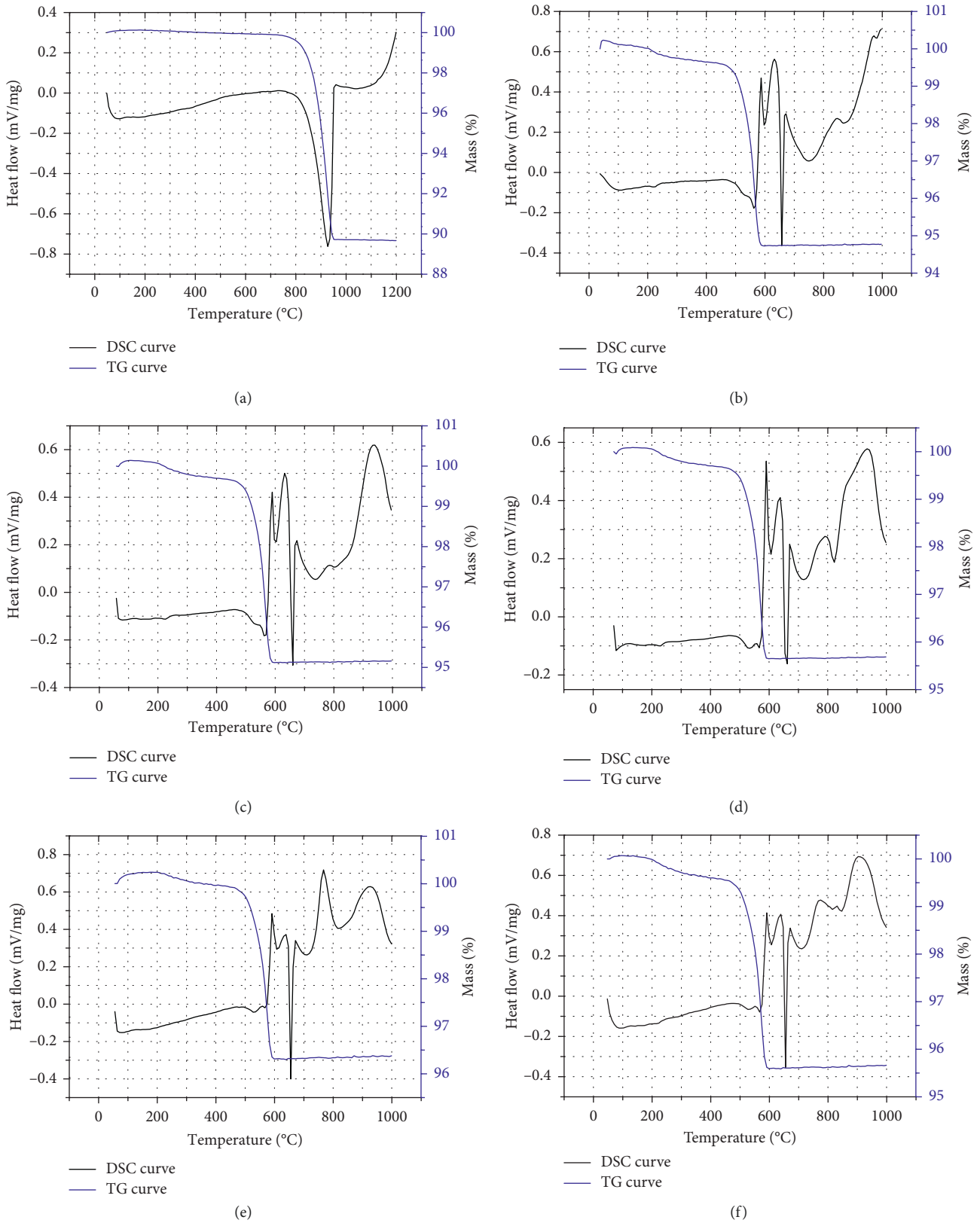

Figure 7: TG-DSC curves of different samples. (a) 0#. (b) 1#. (c) 2#. (d) 3#. (e) 4#. (f) 5#.

Table 4: The parameters for different processes of heat release in the DSC curves.

No.	Heat release (J/g) (0°C~620°C)	Heat release (J/g) (620°C~680°C)	Heat release (J/g) (680°C~1000°C)	Heat release (J/g) (0°C~1000°C)
1#	60.3	−15.8	92.9	137.4
2#	56.8	−14.7	82.7	124.8
3#	53.5	−14.2	54.2	93.5
4#	51.7	−13.3	53.1	91.5
5#	47.4	−11.4	51.2	87.2

well. Enthalpy decreased gently as the temperature increased from 0°C to 600°C, where the enthalpy change less than 10 kJ and the decreasing rate (slope) of about 0.017 kJ/°C could be calculated. When the temperature rose to 600–700°C, a sudden increase of about 25 kJ occurred to the absolute value of enthalpy. This could be attributed to the melting of aluminum over 660°C, the proposed melting point for aluminum according to the literature [19], which released a certain amount of heat due to phase transition into liquid and thus contributed to the increment in absolute value of enthalpy change. At temperature up to 700~1000°C, the absolute value of enthalpy change decreased slightly, for the decomposition of MnO_2 into Mn_2O_3 at 530–940°C would absorb part of the released heat. Since CuO would melt at ~1026°C, the resultant heat release would be embodied by the uptrend of thermograms; particularly, another exothermic band at 1200–1300°C could be observed on the curves corresponding to samples with high CuO content, i.e., 4# and 5#. Finally, when the temperature was higher than 1300°C, the absolute values of enthalpy change in different samples got very close to each other due to the reduced CuO content and the subsequent weakened CuO effect.

Given that other parameters, such as particle size and purity, were controlled at similar values, analytical data in the above comparison possess certain reference values.

3.3. FE-SEM Analysis. Samples with CuO content at 0, 5%, 10%, 15%, and 20% were observed by FE-SEM with 10,000-time magnification, and the micrographs are presented in Figure 6. As can be seen, smaller balls with smooth surface are aluminum powder (particle size of ~1 μm or less) while larger spheres with uneven surface belong to copper oxide particles (particle size of ~1 μm or above). In addition, manganese dioxide is identified as solid-state bulk and flake (particle size of ~5 μm). After ultrasonic oscillation, both aluminum and copper oxide were found wrapping around manganese dioxide, and the whole system became more agglomerated consequently. In terms of the composition variation, the percentage content of aluminum changed little, while manganese dioxide was replaced partially by copper oxide as reflected by the decrease in bulk and flake solids along with the increase in concave and convex spheroids.

3.4. Thermal Property Analysis. In Figure 7, the TG-DSC curve 0# is assigned to neat CuO while curves 1#–5# correspond to samples 1#–5#, respectively. Exothermic regulation was adopted throughout the experiments.

Curve 0# suggested the occurrence of 10.02% mass loss from 748.6 to 942.2°C, which was interpreted by CuO generating Cu_2O with O_2 release during the measurement. While a little gas produced by partial decomposition of MnO_2 would exert trivial influence on the whole reaction, the huge amount of gases from CuO decomposition could intensify the system pressure and subsequently accelerate the flame ejection to a great extent. To further elucidate the gas effect on reaction system, Al/CuO reagent was set up for combustion experiment for comparison; DDT phenomenon was observed, which thus verified gases' enormous impact on flame ejection.

Endothermic peaks at about 500–550°C on DSC curves for 1#–5# were ascribed to MnO_2 decomposition, which happened at 535°C according to the literature [20]. Then, the general exothermic peaks showing up between 600°C and 780°C resulted from the heat release of Al/MnO_2, which embraced two endothermic peaks—the first at around 600°C was generated by heat absorption during MnO_2 decomposing into Mn_2O_3 while the second at 620–630°C came from Al melting [21]. When the reaction temperature reached 720–1000°C, heat release was basically attributed to Al/CuO or Al/Cu_2O, and the included endothermic peak was associated with CuO decomposition process similar to the pattern of 0# TG-DSC curve. In summary, the addition of CuO into Al/MnO_2 system could bring about more intense exothermic behavior at the higher temperature region around 900°C. It would favor the general reaction, for the Al/MnO_2 system can only react at 1500°C or higher. The parameters for different processes of heat release could be found in Table 4.

With the increase of the mass of CuO, both the heat release (0°C to 620°C; 680°C~1000°C; 0°C~1000°C) and the value of the endothermic (620°C~680°C) had decreased gradually.

4. Conclusions

When adding CuO to the high-energy combustion agent of Al/MnO_2 system, the overall combustion reaction would be greatly accelerated and the combined system exhibited an improved ability to melt the steel plate. Based on the experiments of samples 1#–5# and the following analyses, it was found that CuO addition would reduce the combustion heat during the whole reaction process, and the overall reaction rate also declined according to the theoretical calculation. Besides, there was too little difference in particle morphology to exert observable effects. Nevertheless, CuO would still impact the overall reactions positively and significantly, which could be explained by the following two reasons:

(1) The addition of CuO into the Al/MnO_2 system would increase dramatically the gas content throughout the whole reaction. This was greatly conducive to improving the pressure and speed of flame injection so as to accelerate the overall reaction rate and enhance the penetration ability.

(2) The initial temperature of Al/CuO reaction was relatively high, and the heat release at high-temperature region due to CuO addition contributed to the continuous exothermic reaction to a great extent.

Nonetheless, it should be noted that excessive addition of CuO would incur the DDT phenomenon, for the higher reaction rate caused by highly reactive CuO produced oxygen much faster than it could be released. Usage safety of the reagents would be largely compromised. Therefore, the dosage of CuO cannot be increased blindly.

Data Availability

The data used to support the findings of this study are available from the corresponding author upon request.

Conflicts of Interest

The authors declare that there are no conflicts of interest regarding the publication of this paper.

Acknowledgments

This work was supported by the National Natural Science Foundation (project nos. 51673213 and 51505498).

Supplementary Materials

Samples with CuO content at 0, 5%, 10%, 15%, and 20% were observed by FE-SEM with 10,000-time magnification, and the micrographs are presented in these five pictures. These data are about Gibbs's free energy and reaction enthalpy changes. According to Arrhenius formula and Eyring–Polanyi equation, the reaction rate of components can be qualitatively described by Gibbs free energy, and the reaction heat of components can be quantitatively analyzed by enthalpy changes of reaction according to the first law of thermodynamics. Considering the data of Gibbs's free energy and reaction enthalpy changes, the formula can be screened. Thermal properties were analyzed by TG-DSC (NETZSCH STA 449F3, Germany). Samples weighed about 15–25 mg were loaded in a corundum crucible and heated from 20°C to 1000°C at the heating rate of 10°C·min^{-1} under argon protection. DSC is the curve of the reaction heat while the TG is the curve of the sample quality during the reaction. The 0# sample is Al/CuO binary component while the 1–5# samples are Al/MnO_2/CuO. The contents of CuO are 0, 5%, 10%, 15%, and 20%, respectively. The regulation is upward for the exothermic direction. (*Supplementary Materials*)

References

[1] T. Bazyn, P. Lynch, H. Krier, and N. Glumac, "Combustion measurements of fuel-rich aluminum and molybdenum oxide nano-composite mixtures," *Propellants, Explosives, Pyrotechnics*, vol. 35, no. 2, pp. 93–99, 2010.

[2] Z. He, W. U. Shen, and H. Wang, "Thermodynamics analysis of Al_2O_3, TiB_2/Al composites fabricated by exothermic dispersion method," *Chinese Journal of Nonferrous Metals*, vol. 12, no. 3, 2001.

[3] A. N. Ali, S. F. Son, M. A. Hiskey, and D. L. Naud, "Novel high nitrogen propellant use in solid fuel micropropulsion," *Journal of Propulsion & Power*, vol. 20, no. 1, pp. 120–126, 2012.

[4] Y Xu-dong, K Cheng-ping, and D.-Y. Song, *Thermal-Melting Welding Flux and Heat-Release Fusion Welding Flux formed thereby: CN, CN 1295055 C*, Beijing Industrial Press, Beijing, China, 2007.

[5] H. Wang, G. Jian, G. C. Egan, and M. R. Zachariah, "Assembly and reactive properties of Al/CuO based nanothermite microparticles," *Combustion and Flame*, vol. 161, no. 8, pp. 2203–2208, 2014.

[6] S. Wang, W. T. Xin, L. F. Qu, and Y. Y. Wu, "Study on cutting process of manual thermite cutting technology," *Advanced Materials Research*, vol. 621, pp. 211–215, 2013.

[7] M. A. Ilyushin, I. V. Tselinsky, I. A. Ugryumov, V. Y. Dolmatov, and I. V. Shugalei, "Study of submicron structured energetic coordination metal complexes for laser initiation systems condensed phase leading reaction," *Central European Journal of Energetic Materials*, vol. 2, no. 1, pp. 21–33, 2005.

[8] J. P. Shen, X. H. Duan, Q. P. Luo et al., "Preparation and characterization of a novel cocrystal explosive," *Crystal Growth & Design*, vol. 11, no. 5, pp. 1759–1765, 2011.

[9] K. B. Plantier, M. L. Pantoya, and A. E. Gash, "Combustion wave speeds of nanocomposite Al/Fe_2O_3: the effects of Fe_2O_3 particle synthesis technique," *Combustion and Flame*, vol. 140, no. 4, pp. 299–309, 2005.

[10] J. Sun, M. L. Pantoya, and S. L. Simon, "Dependence of size and size distribution on reactivity of aluminum nanoparticles in reactions with oxygen and MoO_3," *Thermochimica Acta*, vol. 444, no. 2, pp. 117–127, 2006.

[11] N. W. Piekiel, C. J. Morris, W. A. Churaman, M. E. Cunningham, D. M. Lunking, and L. J. Currano, "Combustion and material characterization of highly tunable on-chip energetic porous silicon," *Propellants, Explosives, Pyrotechnics*, vol. 40, no. 1, pp. 16–26, 2015.

[12] D. K. Kim, J. H. Bae, M. K. Kang, and H. J. Kim, "Analysis on thermite reactions of CuO nanowires and nanopowders coated with Al," *Current Applied Physics*, vol. 11, no. 4, pp. 1067–1070, 2011.

[13] A. Prakash, A. V. Mccormick, and M. R. Zachariah, "Synthesis and reactivity of a super-reactive metastable intermolecular composite formulation of Al/$KMnO_4$," *Advanced Materials*, vol. 17, no. 7, pp. 900–903, 2005.

[14] N. N. Zhao, C. C. He, J. B. Liu et al., "Preparation and characterization of superthermite Al/MnO_2 and its compatibilities with the propellant components," *Chinese Journal of Explosives & Propellants*, vol. 35, no. 6, pp. 32–36, 2012.

[15] J. X. Song, X. Fang, T. Guo et al., "Thermal properties and kinetics of Al/α-MnO_2 nanostructure thermite," *Journal of the Brazilian Chemical Society*, vol. 29, no. 2, 2017.

[16] Z. Qiao, J. Shen, J. Wang et al., "Fast deflagration to detonation transition of energetic material based on a quasi-core/shell structured nanothermite composite," *Composites Science and Technology*, vol. 107, pp. 113–119, 2015.

[17] E. Weigold, S. T. Hood, and I. E. Mccarthy, "Structure of inert gases from the (e, 2e) reaction," *Physical Review A*, vol. 11, no. 2, pp. 566–575, 1975.

[18] M. Schwaab and J. C. Pinto, "Optimum reference temperature for reparameterization of the Arrhenius equation. Part 1: problems involving one kinetic constant," *Chemical Engineering Science*, vol. 62, no. 10, pp. 2750–2764, 2007.

[19] J. E. Lee, D. H. Bae, W. S. Chung, K. H. Kim, J. H. Lee, and Y. R. Cho, "Effects of annealing on the mechanical and interface properties of stainless steel/aluminum/copper clad-metal sheets," *Journal of Materials Processing Technology*, vol. 187-188, no. 3, pp. 546–549, 2007.

[20] J. Yoo, Y.-H. Lee, B.-H. Seo, Y.-K. Oh, I.-S. Kim, and J. Song, "Dielectric and piezoelectric properties of MnO_2-added non-stoichiometric $(K_{0.5}Na_{0.5})_{0.97}(Nb_{0.96}Sb_{0.04})$ O_3 ceramics," *Journal of the Korean Physical Society*, vol. 57, no. 4(1), pp. 959–962, 2010.

[21] F. Jiao, A. Harrison, A. Hill, and P. G. Bruce, "Mesoporous Mn_2O_3 and Mn_3O_4 with crystalline walls," *Advanced Materials*, vol. 19, no. 22, pp. 4063–4066, 2010.